24th COBEM - 2017

24th ABCM International Congress of Mechanical Engineering
December 3-8, 2017, Curitiba, PR, Brazil

COBEM-2017-0690
EXPERIMENTAL ASSESSMENT OF A LOW REYNOLDS NUMBER VEHICLE

Daniel Acevedo-Giraldo
Laura Botero-Bolívar
Pedro David Bravo-Mosquera
Hernán Darío Cerón-Muñoz
Fernando M. Catalano

Laboratory of Aerodynamics (LAE), Aeronautical Engineering Department
São Carlos School of Engineering - University of São Paulo (EESC-USP) - Av. Trab. São-Carlense, 400. São Carlos, Brazil
daniel.acevedogi@usp.br, laura.boterobol@usp.br, pdbravom@usp.br, hernan@sc.ups.br, catalano@sc.usp.br

Abstract. *This paper reports wind tunnel tests of a low Reynolds number vehicle model. The experiments were conducted at* 1.5×10^5 *Reynolds number (Re). A Laminar Separation Bubble (LSB) was observed on the upper surface of the wing. Such a phenomenon, that occurs at low Reynolds numbers, is caused by the inability of the laminar flow to complete the transition to turbulent attached to the surface of the airfoil, therefore the laminar flow separates before its transition. The lift coefficient (*C_L*) decreased and the drag coefficient (*C_D*) increased by the presence of the bubble, modifying aircraft performance considerably. To guarantee the transition, two processes were carried out. On the first one, a trip was added on the upper surface and as a second alternative, the effective Reynolds number was increased. The results showed how the bubble affects the vehicle performance. Experiments were conducted at the aircraft laboratory of aerodynamics (LAE) of the São Carlos School of Engineering - University of São Paulo (EESC-USP), Brazil.*

Keywords: *High-lift low Reynolds number airfoil, laminar separation bubble, Eppler 423 airfoil, wind tunnel tests.*

1. INTRODUCTION

The airfoil design depends on the purpose of the airfoil as well as on the Reynolds regime that the airfoil will operate. The geometry of the airfoil defines the pressure distribution on the surface, lift distribution, transition and separation aspects. Figure 1 shows two airfoils to different purposes. As can be seen in Fig.1, airfoils for high lift and low Reynolds have a greater camber than high speed airfoils, due to they have to create a larger pressure difference between upper and lower surfaces to compensate the low velocity (Lissaman, 1983).

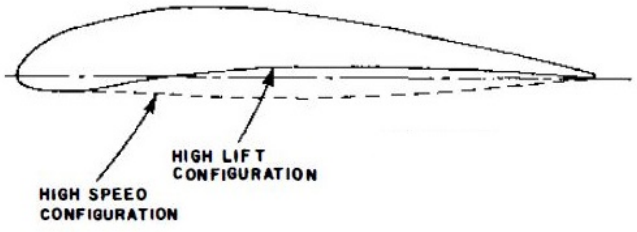

Figure 1. Different purpose airfoils
Reference: Lissaman (1983)

According to Miley (1982), there are three ways to generate lift. The first one is through low pressure on the upper surface, requiring a strong adverse pressure gradient. The second one is using a combination of low pressure on the upper surface and high pressure on the lower surface. Finally, the third way is producing lift from high pressure on the lower surface. Figure 2 presents the different pressure distribution and characteristic airfoil shape for each principle mentioned above. In agreement with Fig.1 and Fig.2, high-lift low Reynolds number airfoils are commonly like the third type.

High-lift low Reynolds number airfoils are typically used on vehicles that require the transport of heavy payload, take off and landing in short distances and flying at low velocity and at high altitude, as well as, propellers and wind turbines (Lin and Pauley, 1996). Figure 3 shows different airfoils applications in function of the Reynolds number.

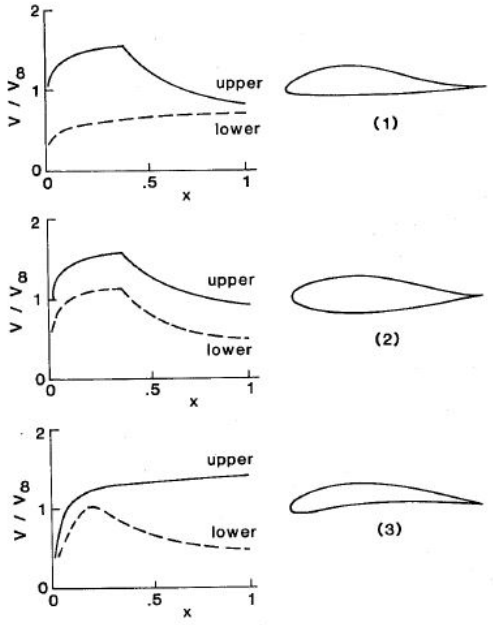

Figure 2. Combination of pressure distribution and airfoil shape
Reference: Miley (1982)

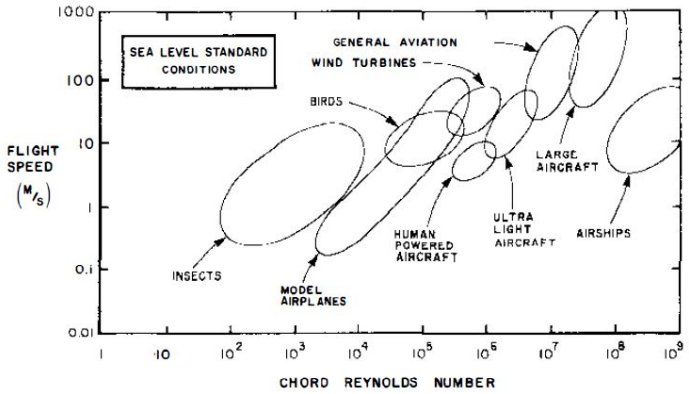

Figure 3. Reynolds number spectrum
Reference: Lissaman (1983)

If the surface of the airfoil is smooth, the free-stream turbulence is low and the Reynolds number is also low, the boundary layer of the airfoil may be completely laminar, this point is known as low critical Reynolds number. Laminar Boundary layer (LBL) causes low friction force whereas turbulent boundary layer (TBL) causes large friction force, however LBL is less stable than TBL. The stability of the LBL depends on both pressure gradient and on the Reynolds number. When subjected to an adverse pressure gradient (increasing pressure), the laminar boundary layer may react in three ways: it may separate and produce stall, separate and reattach shortly thereafter as a turbulent boundary layer, or destabilize and become turbulent. The second case is the most complicated among the three (Miley, 1982).

All airfoils have regions of favorable pressure gradient, where is produced an acceleration of the flow. This higher speed flow has to return to the free-stream velocity at trailing edge, causing an adverse pressure gradient. When the airfoil is operating at high Reynold number, this adverse pressure gradient typically occurs after the transition point, then a TBL could support severe adverse pressure gradient without separation. Nevertheless, at low Reynolds number, the LBL is unable to support any significant pressure gradient, thus, the boundary layer separates still being laminar. As mentioned above, the LBL could separate and reattach downstream as turbulent layer, this occurs due to the fact of when the LBL separates, rapidly undergoes transition to a turbulent flow, increasing their entrainment and making possible the reattachment as a TBL. Between the separation and reattachment point a recirculation zone is generated, this phenomenon is known as Laminar Separation Bubble (LSB) (Miley, 1982; Lissaman, 1983). Figure 4 shows a schematic view of LSB phenomena, upstream of the bubble the flow is completely laminar, downstream is completely turbulent and the dividing streamline between separation and reattachment point separates the recirculating flow region (with constant pressure) from the separated flow (Pröbsting and Yarusevych, 2015).

According to Roberts (1980) there are two necessary conditions for the formation of LSB: the first one is an adverse pressure gradient greater enough to cause laminar separation and the second one is flow condition over the airfoil such that the boundary layer will be laminar at separation point, i.e. the distance from stagnation to separation point must be shorter than the distance until transition point. Depending on the condition of Reynolds number and free-stream turbulence, the bubble could cause a significant change in the pressure distribution of the airfoil, affecting the suction peak and therefore the lift also, increasing the drag and constraining the maximum possible angle of attack (AoA) (Roberts, 1980; Lissaman, 1983).

High-lift low Reynolds number airfoils, owing to their geometry and their operate regime, usually present LSB phenomena, whence it is necessary to perform a complete study of their behavior at different angles of attack and different Reynolds number, in order to establish their operational limits. Furthermore, knowing the bubble location in the airfoil, it could be avoid forcing the transition upstream of any severe pressure gradient (Miley, 1982; Lissaman, 1983).

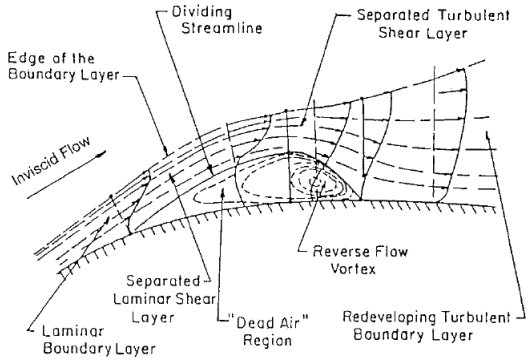

Figure 4. Laminar separation bubble
Reference: Lin and Pauley (1996)

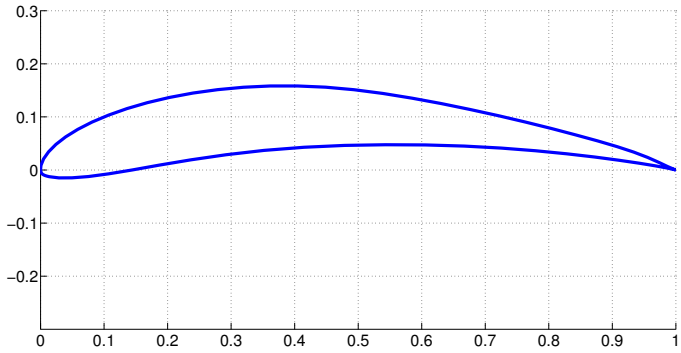

Figure 5. Eppler 423 airfoil

The airfoil Eppler 423, shown in Fig. 5, is a high-lift low speed wing airfoil. It has a higher camber compared with most of 4-digit NACA airfoils and is characterized by a high $C_{L_{max}}$, C_d in cruise comparable to other airfoils and a soft stall; it is usually used in model airplanes and wind turbines. This airfoil belongs to the third category of Fig. 2 and usually presents LSB at low Reynolds number (McStravick *et al.*, 2010).

This research reports wind tunnel tests of an unmanned Aerial Vehicle (UAV) scale model, which use Eppler 423 as wing airfoil. The UAV was designed for superficial volcano monitoring at a Reynolds number of $Re = 3 \times 10^5$. This kind of mission requires flight at high altitude and low speed in order to take data from the environment, such as gas emission, geographical deformation and inside thermal changes, thus, it is necessary use high lift airfoils. More information about UAV design is founded in Bravo-Mosquera *et al.* (2017).

Experimental tests showed that the UAV presents the LSB phenomena, therefore, visualization methods and aerodynamic balance measures were used to detected bubble behavior. Moreover, analytical analysis through XFOIL (Drela, 1989) were carried out in order to compare the airfoil and the bubble behavior modifying the Reynolds number and turbulence intensity (N_{crit}). Finally, two ways to avoid the bubble were tested, increasing the Reynolds number and forcing the transition trough a roughness of high of $0.8mm$ before the bubble formation.

2. EXPERIMENTAL SET-UP

The experiments were carried out in two stages. The acquisition of the aerodynamic forces was conducted in a closed-circuit wind tunnel that has a working section of $1.30m \times 1.70m \times 3.00m$ (Catalano, 2004). The maximum velocity achieved is about 40 m/s and the turbulence level is 0.21% (Santana *et al.*, 2014). On the other hand, flow visualization experiments were undertaken in a blower wind tunnel with an open working section of $0.8m \times 1.05m$, the operating velocity range is from 10 to $30m/s$. Both tunnels are located at the laboratory of aerodynamics (LAE) of the São Carlos School of Engineering - University of São Paulo (EESC-USP), Brazil. Figure 6 presents the plan view of the closed wind tunnel.

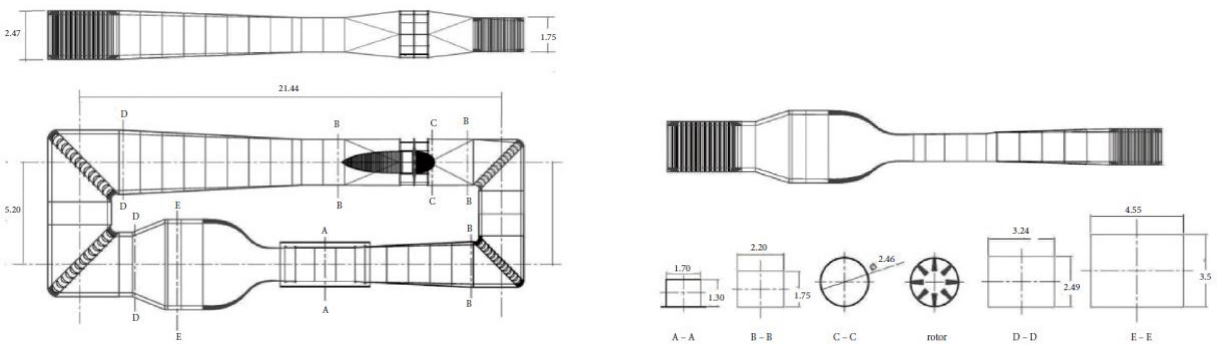

Figure 6. LAE-1 Wind tunnel plan view
Reference: Santana *et al.* (2014)

A half-model was manufactured and its size was defined from the lowest dimension of the blowing tunnel working section. In this way, the main measurements of the model are: mean aerodynamic chord (MAC) of $0.113m$; semi-wing span of $0.6m$ and total length of $1.2m$. The model was constructed with a Cliever CL2 pro plus 3D printer. The

manufacturing material used is Poly-lactic Acid (PLA), which is produced by fermentation of a renewable agricultural source of corn. Besides being a biodegradable material, its mechanical properties are satisfactory for the current purpose (Auras *et al.*, 2003; Dorgan *et al.*, 2000). Eight modular pieces were printed to complete the model using an internal structure honeycomb type. The honeycomb density was higher in the wing than in the fuselage in order to seeking more rigidity on the wing. The size of honeycomb and the thickness of the edge were controlled by 3D printer software according to manufacturer instructions.

Finally, the velocity was fixed at $23m/s$, which corresponds to a Reynolds number of 1.5×10^5. Atmospheric conditions measured at wind tunnels location were $\rho = 1.079Kg/m^3$, $\mu = 1.907 \times 10^5 Pa.s$, $T = 24°C$ and $P = 92KPa$.

2.1 Aerodynamic balance experiments

In these experiments the test model was vertically mounted at the center of the test section (Fig. 7). Aerodynamic measurements were performed with a balance of three D.O.F. The data is acquired through a HBM module, that allows gain and filtering regulations and which was set to take 5000 samples with a frequency sample of 500 samples per second. The accuracies related to lift, drag and pitch are $0.01N$, $0.01N$ and $0.01N - m$ respectively. The angle of attack has an accuracy of $0.1deg$.

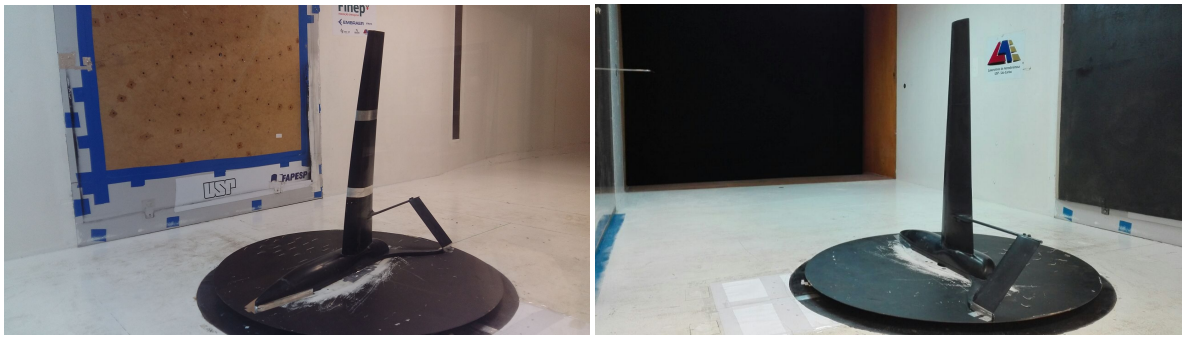

Figure 7. UAV in the closed wind tunnel
Reference: Bravo-Mosquera *et al.* (2017)

2.2 Flow visualization

The flow visualization technique used is known as surface oil-flow (Fig. 8), which enables the observation of the boundary layer flow in wind tunnel easily and quickly (Ristić, 1820). In this technique the model surface is coated with a mixture of a vegetable oil and fine pigment, indicating the pattern of the flow on the surface. The technique allows the observation of the lines of separation and reattachment of the flow.

Figure 8. UAV in the blower wind tunnel

3. RESULTS

Numerical simulations of the Eppler 423 airfoil were performed in XFOIL free code program (Drela, 1989) . In this section, The effects of the Reynolds number variation as well as the N_{crit} factor are analyzed. N_{crit} is the parameter used to relate the disturbance level in which the airfoil operates and its effects are highly relevant to the results of the transition behavior. XFOIL is a panels method program that uses the e^n criterion to calculate the transition. N_{crit} varies from 1 to 9, where $N_{crit} = 1$ is equivalent to 1.966% and $N_{crit} = 9$ to 0.07% (Drela and Youngren, 2001).

The distribution of the pressure coefficient is an important tool to analyze the aerodynamic characteristics of the airfoil where the stagnation point, the suction peak, separation and even the phenomenon of the presence of bubbles can be observed. LSB is identified whether there is a region, between two pressure gradients, where the Cp is constant. Figure 9 presents a typical pressure distribution where there is a bubble and some important points are being indicated. The bubble may be formed on the upper surface as well as on the lower, even though, on the upper surface is always greater due to the greater adverse pressure gradient.

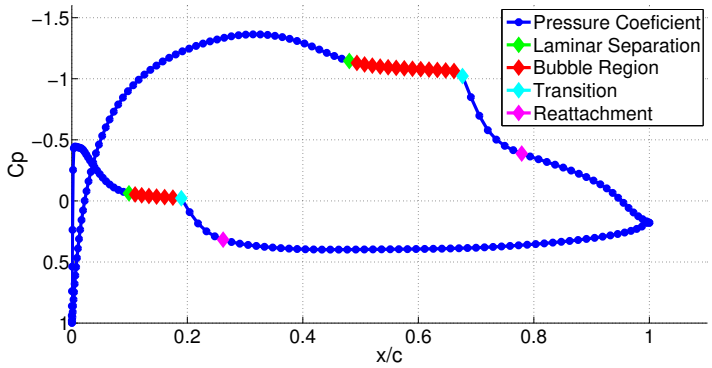

Figure 9. Typically pressure distribution with LSB

Figure 10 shows the difference between pressure distribution on the Eppler 423, varying the N_{crit}. As can be seen, when the level of disturbance is lower, the length of the bubble will be greater, until $N_{crit} = 1$ where no bubble is observed. In this case, because of the increase in the turbulence level, the boundary layer is able to complete its natural transition before to the separation. The effects of the Reynolds number on the bubble can be seen in the figure 11. The length of the bubble decreases when the Reynolds number is increased. Whether the Reynolds number is sufficiently high, even with low free stream turbulence level ($N_{crit} = 9$), the bubble is not generated, due to the flow has enough kinetic energy to make the transition and remain attached to the surface.

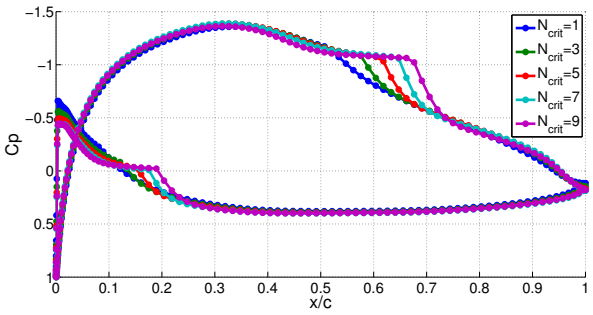

Figure 10. Pressure distribution at $Re = 1.5 \times 10^5$ and $\alpha = 0$

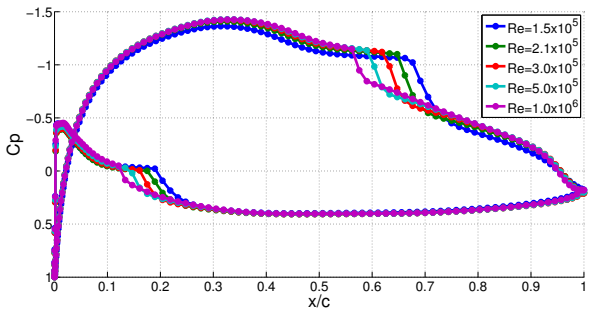

Figure 11. Pressure distribution at $N_{crit} = 9$ and $\alpha = 0$

Figure 12 - 15 shows the C_l vs α and C_d vs α curves, varying the N_{crit} and the Reynolds number. In all cases, the airfoil presents a soft stall and the linear region does not change significantly. However, there are some variations in each case. As the Reynolds number increase the $C_{l_{max}}$ also increases, due to the fact that the flow has more energy to remain attached to the body. C_d decreases because the viscous forces become weak, then the boundary layer thickness is reduced.

The increase of the $C_{l_{max}}$, when the N_{crit} was reduced, is related to the formation of bubbles. After the maximum suction, there is a region of constant pressure where the bubble is formed. The larger the bubble is, the longer this region of C_p constant will be, increasing the area under the C_p curve and consequently the lift coefficient. The latter is only true when the suction peak is not affected by the bubble. When the bubble is formed before the suction peak or it is larger enough not to allow the formation of a suction peak, the lift coefficient is reduced. In addition, in all cases of bubble formation, the drag is increased, because the airfoil and the bubble work as a single body so that the boundary layer passes outlining the bubble, increasing the profile drag.

XFOIL analyzes this kind of phenomena keeping the same calculation procedure before the separation point; modifying N_{crit}, XFOIL recalculate the transition point, although does not recalculate the suction region, this can be appreciated in fig 10, where the pressure distribution is always the same except in the bubble region (Drela and Youngren, 2001).

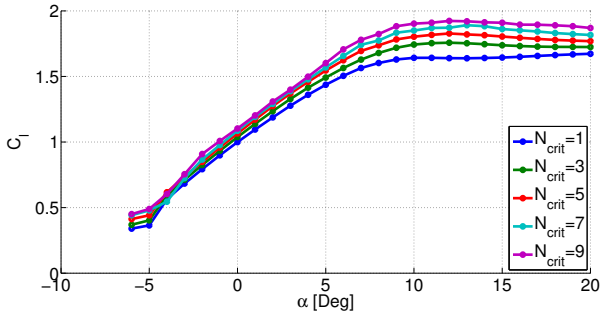

Figure 12. Lift coefficient at $Re = 1.5 \times 10^5$

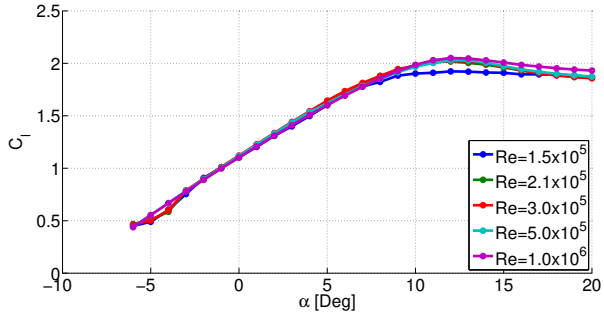

Figure 13. Lift coefficient at $N_{crit} = 9$

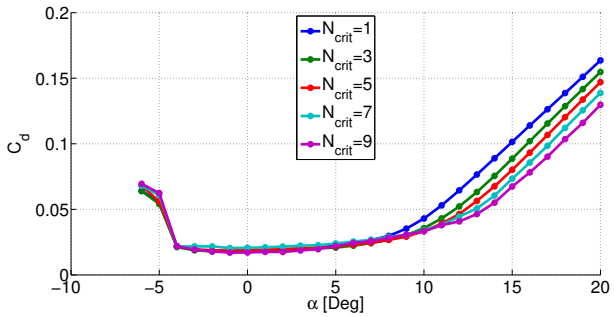

Figure 14. Drag coefficient at $Re = 1.5 \times 10^5$

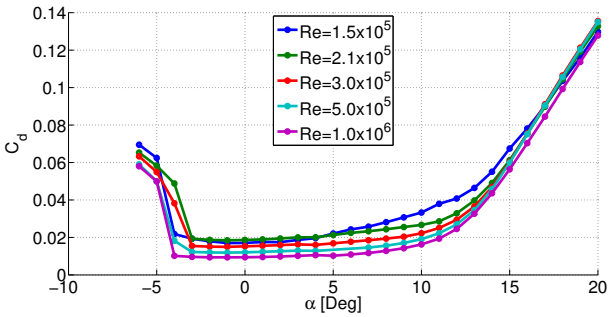

Figure 15. Drag coefficient at $N_{crit} = 9$

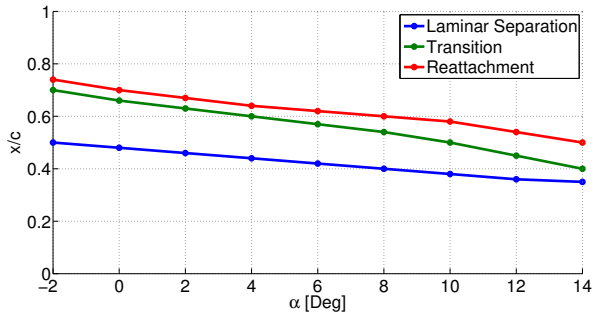

Figure 16. Bubble displacement at $Re = 1.5 \times 10^5$ and $N_{crit} = 9$

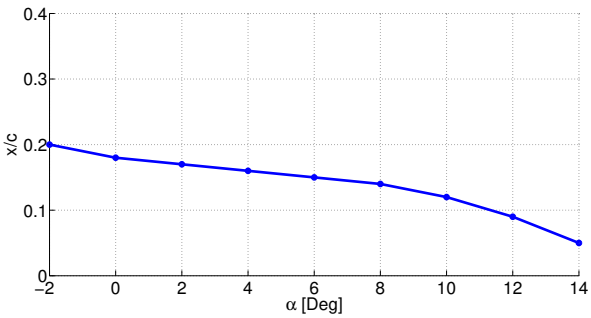

Figure 17. Bubble length at $Re = 1.5 \times 10^5$ and $N_{crit} = 9$

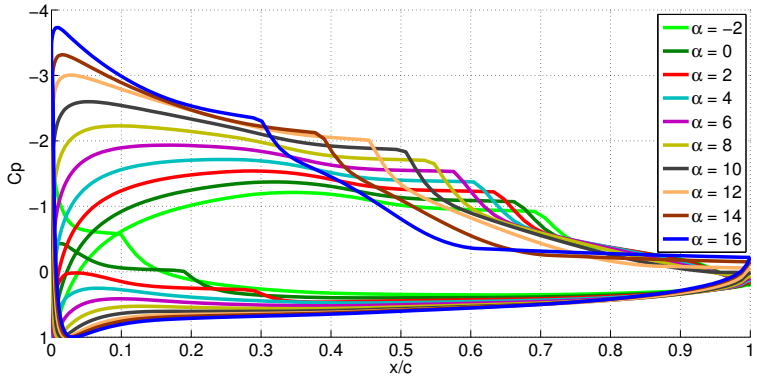

Figure 18. Pressure distribution at $Re = 1.5 \times 10^5$ and $N_{crit} = 9$

Figures 16, 17 and 18 show how the bubble is moving toward the leading edge and is decreasing its length as increasing the AoA; this occurs insomuch as the laminar separation is closer to the suction peak and the larger pressure gradient amplifies any perturbation in the LBL, resulting in earlier transition in the free shear layer (Roberts, 1980). In this case, at $AoA = 14°$, the laminar separation and the transition are coincident, at any AoA greater than $14°$, transition will occur upstream of separation point and the bubble will no longer exist.

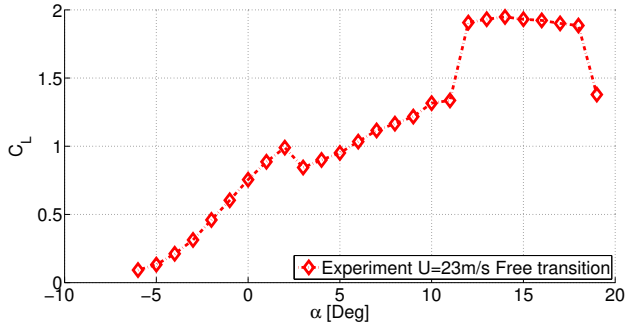

Figure 19. Lift coefficient with LSB

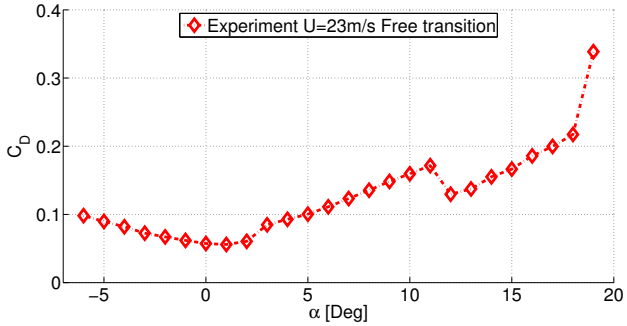

Figure 20. Drag coefficient with LSB

Figures 19 and 20 show the C_l vs α and C_d vs α curves obtained experimentally. There is a severe decrease of lift and increase of drag between $\alpha = 3°$ to $\alpha = 11°$, this is due a LSB phenomena on the upper surface; above $\alpha = 11°$ the kinetic energy of the fluid increases and promotes the transition from laminar to turbulence flow prior to the separation of the boundary layer and the aircraft behavior become back to the normal behavior.

Indeed, through the visualization experiments, the presence of a bubble in this range of angles of attack was verified; e.g. at $\alpha = 0°$ a bubble is formed approximately at 25% of MAC with a length of 3 cm approximately, (25% of MAC), as can be observed on Fig. 8.

Unlike the numerical analysis, the lift coefficient was not increased. As can be seen in the figures 10 and 11, the Eppler 423 airfoil presents its suction peak between $x/c = 0.3$ and $x/c = 0.4$ and the bubble appears at $x/c = 0.25$, thereby the bubble affects the typical generation of the suction peak.

To avoid the formation of the bubble, two alternatives were considered. The free-stream velocity was increased, raising the Reynolds number and, on the other hand, a roughness at 25% of MAC was set. Both of them avoided the LSB and there was no such abrupt decrease in c_L values in the range $3° < \alpha < 11°$, see Fig. 21 and 22. This occurs on account of in both cases the transition is before the separation point, in the first case due to the increase of the flow kinetic energy and on the second case due to the forced transition before the separation.

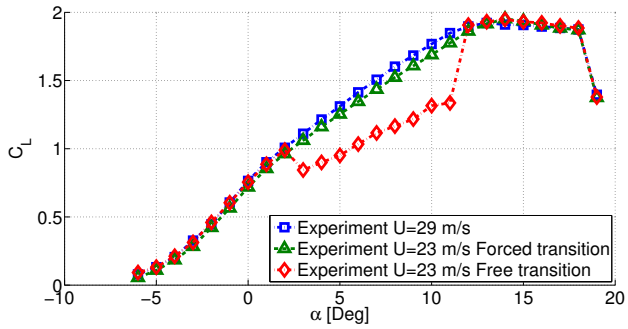

Figure 21. Lift coefficient

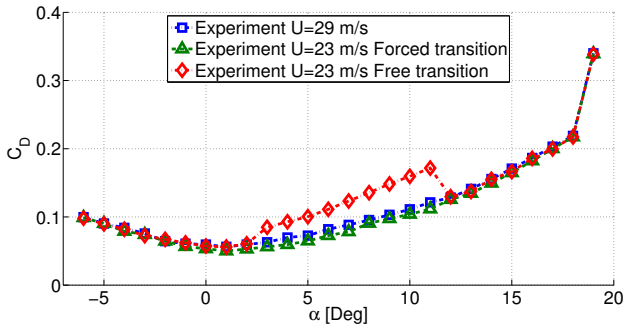

Figure 22. Drag coefficient

To define the roughness, the bubble feature observed in flow visualization at 11° was considered. It was defined the separation point and the roughness was located before to guarantee the transition.

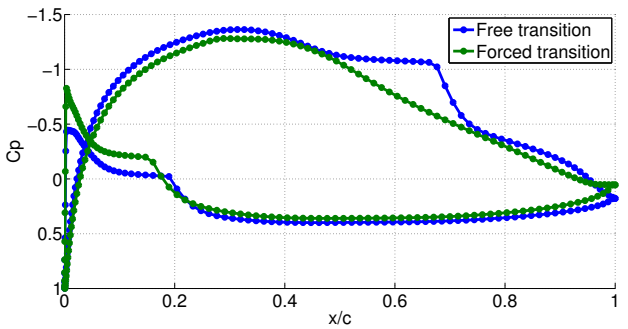

Figure 23. Pressure distribution with free and forced transition

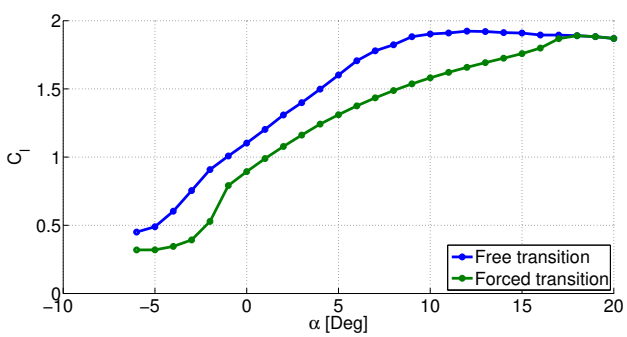

Figure 24. Lift coefficient with free and forced transition

Figure 23 shows XFOIL simulation at $Re = 1.5 \times 10^5$, $N_{crit} = 9$ and $AoA = 0$ with free transition and forced transition at 25% of MAC, which represents the trip on the real model. With forced transition model, the pressure distributions does not present bubble phenomena, however reduce the suction peak. Figure 24 presents the phenomena commented above, where the lift increased with free transition is due to the constant pressure region caused by the bubble.

4. CONLCUSIONS

High-lift low Reynolds number airfoils present grater advantages in both civil and military applications, however they are liable to present bubble phenomena due to their laminar boundary layer, then it is important to analyze completely the behavior of the wing or airfoil in order to know in which conditions of angle of attack, velocity and turbulence intensity the aircraft could operate. In conditions in which the bubble is formed, the aircraft could not be operated.

Wind tunnel experiments (balance and flow visualization) of UAV with LSB phenomena were carried out. The XFOIL simulations also served as method to verify and evaluate the characteristics of LSB phenomena. The results obtained with analytical and experimental methods showed that the bubble is avoid using the trip or increasing the velocity. Before the bubble formation or after its destruction, the behavior of the vehicle is the same for all arrangement.

According to the results obtained, the UAV could carry out missions in high turbulence environments. In this case, the high energy level on the boundary layer would cause the natural transition.

5. REFERENCES

Auras, R.A., Harte, B., Selke, S. and Hernandez, R., 2003. "Mechanical, physical, and barrier properties of poly (lactide) films". *Journal of plastic film & sheeting*, Vol. 19, No. 2, pp. 123–135.

Bravo-Mosquera, P.D., Botero-Bolivar, L., Acevedo-Giraldo, D. and Cerón-Muñoz, H.D., 2017. "Aerodynamic design analysis of a uav for superficial research of volcanic environments". *Aerospace Science and Technology*.

Catalano, F., 2004. "The new closed circuit wind tunnel of the aircraft laboratory of university of sao paulo, brazil". In *24TH International Congress of the Aeronautical Sciencies ICAS*.

Dorgan, J.R., Lehermeier, H. and Mang, M., 2000. "Thermal and rheological properties of commercial-grade poly (lactic acid) s". *Journal of Polymers and the Environment*, Vol. 8, No. 1, pp. 1–9.

Drela, M., 1989. "Xfoil: An analysis and design system for low reynolds number airfoils". In *Low Reynolds number aerodynamics*, Springer, pp. 1–12.

Drela, M. and Youngren, H., 2001. "Xfoil 6.94 user guide".

Lin, J.M. and Pauley, L.L., 1996. "Low-reynolds-number separation on an airfoil". *AIAA journal*, Vol. 34, No. 8, pp. 1570–1577.

Lissaman, P., 1983. "Low-reynolds-number airfoils". *Annual Review of Fluid Mechanics*, Vol. 15, No. 1, pp. 223–239.

McStravick, D.M., Houchens, B.C., Garland, D.C. and Davis, K.E., 2010. "Investigation of an eppler 423 style wind turbine blade". In *ASME 2010 4th International Conference on Energy Sustainability, ASME, Phoenix, AZ, USA*.

Miley, S.J., 1982. "A catalog of low reynolds number airfoil data for wind turbine applications".

Pröbsting, S. and Yarusevych, S., 2015. "Laminar separation bubble development on an airfoil emitting tonal noise". *Journal of Fluid Mechanics*, Vol. 780, pp. 167–191.

Ristić, S., 1820. "Flow visualization techniques in wind tunnels–optical methods (part i)". *Scientific Technical Review, ISSN*, Vol. 206, p. 2007.

Roberts, W., 1980. "Calculation of laminar separation bubbles and their u oc.-af effect on airfoil performance 2 & oo y". *AIAA journal*, Vol. 18, No. 1.

Santana, L.D., Carmo, M., Catalano, F.M. and Medeiros, M.A., 2014. "The update of an aerodynamic wind-tunnel for aeroacoustics testing". *Journal of Aerospace Technology and Management*, Vol. 6, No. 2, pp. 111–118.

6. RESPONSIBILITY NOTICE

The authors are the only responsible for the printed material included in this paper.